Nanomed J. 10(3): 1-17, Summer 2024

RESEARCH PAPER

Green synthesis, characterization, and evaluation of antimicrobial and antioxidant activities of CuO, Co_3O_4, and CuO-Co_3O_4 Nano system using *Moringa stenopetala* plant leaf extracts

Desalegn Tesfa Tefera [1], Tegene Desalegn Zeleke [1]*

[1]Adama Science and Technology University, School of Applied Natural Science, Department of Applied Chemistry, Adama, Ethiopia

ABSTRACT

Objective(s): The purpose of this study was to synthesize copper oxide nanoparticles (CuO NPs), cobalt oxide nanoparticles (Co_3O_4 NPs), and CuO-Co_3O_4 nano system using Moringa stenopetala plant leaf extract. These nanoparticles were specifically developed for their antioxidant and antibacterial properties.

Materials and Methods: The nanoparticles were synthesized by a green synthesis approach using M. stenopetala leaf extract. Comprehensive characterization using spectroscopic techniques such as X-ray diffraction (XRD), UV-visible spectroscopy, scanning electron microscopy (SEM), Fourier transform infrared (FT-IR), and thermogravimetric analysis (TGA) was executed.

Results: UV-Vis analysis revealed an energy bandgap of 3.32 eV for CuO NPs, 3.36 eV for Co_3O_4 NPs, and 3.66 eV for CuO-Co_3O_4 nano system. XRD analysis revealed that CuO NPs have a monoclinic crystal structure with an average crystallite size of 11.59 nm, whereas Co_3O_4 NPs have a cubic crystal structure with an average crystallite size of 12.25 nm. The CuO-Co_3O_4 nano system exhibited an average crystal size of 9.53 nm. The SEM images showed inhomogeneous composition and large granular particles of CuO NPs, inhomogeneous cubic shape and size with encapsulation and hydrogen bonding aggregation of Co_3O_4 NPs, and particle heterogeneity. The CuO-Co_3O_4 nano system. FT-IR analysis confirmed the presence of bioactive molecules such as flavonoids, tannins, terpenoids, steroids, glycosides, saponins, and phenols that actively participate in the synthesis process.

Conclusion: The synthesized CuO-Co_3O_4 nano system showed superior inhibitory effects against the selected bacterial strains compared to CuO NPs and Co_3O_4 NPs. Furthermore, they showed excellent antioxidant activity. These results highlight the significant potential of CuO-Co_3O_4 nano system for a wide range of applications due to their remarkable bacterial inhibition and radical scavenging properties.

Keywords: *Antimicrobial activity, Antioxidant activity, Bacteria, Biosynthesis, Nano system, Phytochemicals*

How to cite this article

Tesfa DT, Zeleke TD. Green synthesis, characterization, and evaluation of antimicrobial and antioxidant activities of CuO, Co_3O_4, and CuO-Co_3O_4 nano system using Moringa stenopetala plant leaf extracts. Nanomed J. 2024; 10(3): 1-17. DOI:

INTRODUCTION

Nanotechnology, an emerging field, involves manipulating objects at incredibly small scales, ranging from a few nanometers to under a hundred nanometers. This size range encompasses various structures found in chemistry, including colloids, micelles, polymer molecules, and phase-separated domains in block copolymers. Fascinatingly, it also encompasses large molecules and assemblies like buckytubes, silicon nanorods, and compound semiconductor quantum dots, which are at the forefront of nanostructure research [1]. Nanotechnology is the creation, manufacturing, and use of structures, devices, and systems through control of size and shape at the nanoscale [2].

Nanomaterials (NMs) have become more popular in the 21st century because of their versatility and ability to be treated as major research focus areas in the sectors of energy, water, and water sanitation [3], medical [4], agriculture [5], material science, and cosmetics. Nanotechnology involves manipulating materials

* *Corresponding author: Email: tegened@yahoo.com*

Note. This manuscript was submitted on December 21, 2023; approved on February 21, 2024

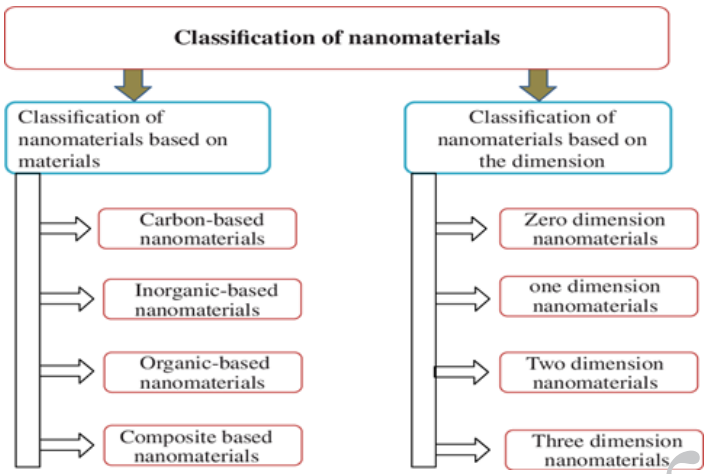

Fig. 1. Classification of nanomaterials

at atomic, molecular, and super molecular levels, utilizing nanomaterials with dimensions of 1-100 nm. The term "nano" originates from the Greek word "Nanos," meaning dwarf, representing one billionth (10^-9) of a meter in diameter. It encompasses structures both larger and smaller than what is typically noticeable (i.e., > 1 nm and ≤ 100 nm) [6].

Researchers classify nanomaterial based on various criteria. Fig. 1 presents classification of nanomaterial based on the constituent materials and sizes of the nanoparticles.

Due to their distinct, flexible, and adaptive properties in optics, mechanics, electronics, biocatalysts, and magnetism, nanomaterials (NMs) have become increasingly significant in technological advancements. The remarkable characteristics of NMs, which can be tailored to specific applications, stem from their large surface area and reduced size. The physical attributes, such as dimensions, configuration, and composition of nanoparticles, greatly influence their reactivity, durability, and other properties, making them highly versatile for a wide range of commercial and residential applications [7]. Metal oxide nanoparticles, including copper oxide (CuO), zinc oxide (ZnO), and titanium dioxide (TiO_2), are among the extensively studied NMs due to their unique qualities and diverse uses [7].

Green nanotechnology, based on the twelve principles of green chemistry, has emerged as an environmentally friendly alternative to conventional nano synthesis methods. Unlike chemical and physical approaches, the biological method for NP synthesis is highly effective and sustainable, avoiding toxic by-products and minimizing harm to the ecosystem [8].

Plant extracts containing biomolecules serve as capping and reducing agents for metal nanoparticle synthesis. This efficient and straightforward method is preferred over using fungi and algae due to the challenges in maintaining their culture media. Thus, utilizing plant extracts for the reduction of metal ions is the preferred approach for producing metal nanoparticles [8].

Plant extracts have diverse properties and applications in multiple industries due to their rich composition of bioactive compounds. These compounds, including flavonoids, phenols, vitamins, and acids, possess potent antioxidant effects. Notable compounds like quercetin, catechins, tocopherol, and chlorogenic acid contribute to the health-promoting properties of plant extracts [9].

Moringa, a tropical plant from the Moringaceae family, includes species like Moringa oleifera and *M. stenopetala*, known for their versatility. Moringa stenopetala, also called the East African Moringa tree, originates from southern Ethiopia and northern Kenya. It is revered with names like "Tree of Life," "Tree that never dies," and "Magic Tree" due to its remarkable properties. Extracts from *M. stenopetala* are utilized as capping and reducing agents in nanoparticle synthesis, capitalizing on the plant's reduction properties for the stability and reduction of metal ions in nanoparticle formation [9]. Therefore, this study was aimed at the green synthesis of CuO NPs, Co_3O_4 NPs, and CuO-Co_3O_4 nano system using an extract from *M. stenopetala* leaves to evaluate their antioxidant and antimicrobial activities against selected bacterial strains.

In previously reported studies, various synthesis methods have been employed for the production of nanoparticles [10]. However, the current study focuses on the synthesis of a unique nano system using green synthesis approach, which involves the utilization of *M. stenopetala* plant leaf extract as a reducing agent. This method offers several advantages over conventional approaches, including its environmentally friendly nature and the potential for producing nanoparticles with distinct properties.

MATERIALS AND METHODS

Chemicals and reagents

In this study, Trihydrate copper nitrate ($Cu(NO_3)_2.3H_2O$, 99.8%), Dimethyl sulfoxide (DMSO), Sodium hydroxide (NaOH, Sigma Aldrich 99% purity), Cobalt (II) nitrate hexahydrate ($CoNO_3.6H_2O$, 99.9%,), Ferric chloride (Sigma Aldrich, 99%, purity), chloroform, sulfuric acid (H_2SO_4, Sigma Aldrich 98% purity), Ethanol (C_2H_5OH 99.8%, Ethiopia), Distilled water. 2, 2-Diphenyl-1-picrylhydrazyl hydrate (DPPH) were used. All reagents were analytical grade and purchased from Addis Ababa, Ethiopia (YESHADAM TRADING PLC, PARACHEM INDUSTRY & TRADING PLC, and ET WISDOM IMPORT & EXPORT PLC) Local market and used without further purification.

Instruments

The instruments that were used for characterizing the synthesized NPs include UV-Vis spectroscopy (UV3600plus, SHIMADZU, Japan), which helped us to study the optical properties of the nanoparticles and nanocomposite, FT-IR (FTIR Perkin Elmer's spectrophotometer), for analysis of the vibrational modes of atoms in the molecules, PXRD (SHIMADZU, XRD-7000S, Japan), to characterize the nature of crystal structure of nanoparticles, SEM (JCM-6000plus BENCH TOP SEM, SHIMADZU Corporation, Japan), was used to study the morphology of the synthesized nanoparticles, and TGA (Differential Thermal gravimetry), DTG-60H, SHIMADZU Corporation, Japan) was used to investigate the thermal stability of the nanoparticles.

Preparation of M. Stenopetala Leaf Extract

The *M. stepenotala* leaves were collected from Adama Science and Technology University campus, Oromia regional state, Ethiopia. The leaves were washed repeatedly with running tap water and rinsed with de-ionized water. The leaves were air-dried for 6 days. The samples were cut into small units and ground with the aid of mortar and pestle. About 10 g of the dry leaf sample was weighed and soaked in 200 mL of de-ionized water and boiled at 80 °C on a hot plate with frequent stirring for 30 min. The extract was cooled and filtered with Whatman no. 1 filter paper. The aqueous extracts were stored in a sealed plastic container at 20 °C [11]. Fig. 2 presents summary of procedure involved in the aqueous extraction of M. stepenotala plant leaves.

Phytochemical analysis of aqueous extract m. stenopetala plant

The plant extract was subjected to assessment for the existence of the phytochemicals by using the following reported standard methods [12].

Tests for flavonoids (Alkaline Reagent Test)

2 mL of 2.0% NaOH mixture was mixed with aqueous plant crude extract; a concentrated

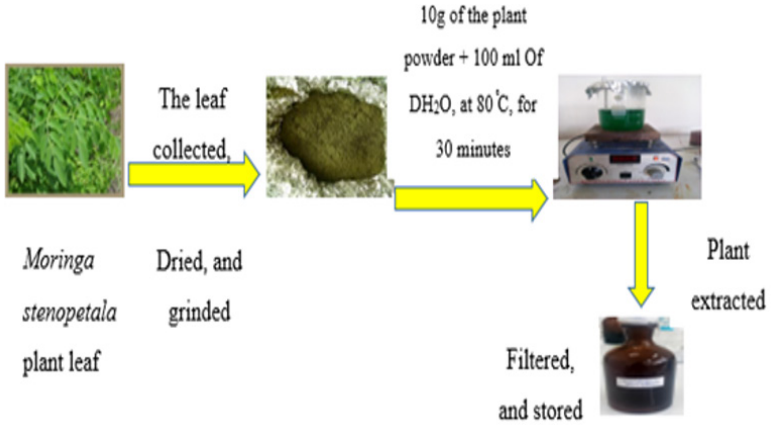

Fig. 2. General procedure for aqueous extraction of M. stenopetala plant leaf

yellow colour was produced, which became colourless when 2 drops of diluted acid were added to the mixture. That result showed the presence of flavonoids.

Test for tannins (Ferric chloride test)

2 mL Plant extract was taken in the test tube and boiled. 5 drops of 0.1% $FeCl_3$ were added and gave a brownish-green or a blue-black colour, which confirmed the presence of tannins.

Test for terpenoids (Salkowski test)

2 mL of aqueous plant extract was mixed with 2 mL of chloroform and 3 mL concentrated H_2SO_4 carefully to form a layer. A reddish-brown coloration of the interface was formed and shows positive results for the presence of terpenoids.

Test for steroids

2 mL of chloroform and concentrated H_2SO_4 were added with the 5 mL aqueous plant crude extract. In the lower chloroform layer, the red colour has appeared that indicating the presence of steroids.

Tests for glycosides (Salkowski's Test)

2 mL concentrated H_2SO_4 was added to the aqueous plant extract.

A reddish-brown colour was formed which indicates the presence of steroidal aglycone part of the glycosides.

Test for phytosterols (Salkowski's test)

2 mL of aqueous plant extract and 10 mL of chloroform were added and then filtered. 5 drops of the concentrated H_2SO_4 were added to the filtrate; the mixture was shaken and examined for the appearance of a golden yellow colour.

Test for saponins

0.5 g of plant extract was taken, then 5 mL of distilled water was added and shaken while heating to boil. Frothing was shown in the presence of saponins.

Test for phenols

5 drops of 2% of $FeCl_3$ were added to 2 mL of aqueous plant extract and the formation of a bluish-green to black colour indicates the presence of phenols.

Procedure for synthesis of CuO nanoparticles

The synthesis of CuO nanoparticles was conducted with a precipitation method [13, 14]. In a typical procedure, summarized in Fig. 3 a stoichiometric amount of 0.2 mol L^{-1} Cu $(NO_3)_2.3H_2O$ was dissolved in 500 mL of distilled water under magnetic stirring; then, 100 mL of *moringa stenopetala* plant aqueous extract was added to 100 mL of the metal salt solution, and the mixture was heated under stirring at 80 °C for 30 min. The solution colour was changed from blue to brown-green. At that temperature, the aqueous solution of NaOH (2 mol L^{-1}) was added dropwise until pH = 11, and the precipitate was observed. The precipitate of the sample was, then, centrifuged at 1000 rpm for 20 min and washed with deionized water and ethanol to remove impurities. Finally, the precipitate was dried in an oven at 80 °C for 4 hr and was ground to a fine powder using an agate mortar. The black powder obtained from the above-mentioned method was calcinated.

Procedure for synthesis of Co_3O_4 nanoparticles

For the fabrication of cobalt oxide NPs, as presented in Fig. 4, freshly prepared plant extract (100 mL) was added to 0.2 M solution (100 mL) of Co $(NO_3)_2.6H_2O$, and this reaction solution was kept on the hot plate for 3 hr at 80 °C to synthesize cobalt oxide nanoparticle. After 3 hr, the solution was transferred into the oven at 100 °C for 5 hr to get the dried precipitate. Further, the precipitate of cobalt oxide NPs was calcinated. Finally, synthesized Co_3O_4 NPs were characterized by spectroscopic and microscopic analysis [15].

Procedure for synthesis of CuO-Co_3O_4 nano system

Synthesis of CuO-Co_3O_4 composite NPs using *M. stenopetala* leaf extract was carried out

Fig. 3. General procedure for the biosynthesis of copper oxide nanoparticles using *M. stenopetala* extract

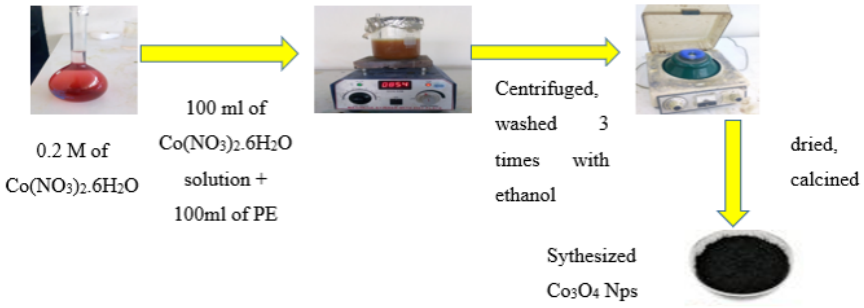

Fig. 4. General procedure for the biosynthesis of cobalt oxide nanoparticles using M. stenopetala extract

according to the literature report with minor modifications. For the synthesis of CuO-Co_3O_4 nano system, as summarized in Fig. 5, 100 mL of 0.2 M Cu $(NO_3)_2.3H_2O$ solution was added to the 1000 mL beaker. Then, 100 mL of 0.2M Co $(NO_3)_2.6H_2O$ solution was added to the beaker while stirring for 15 min. After 15 min, 200 mL of plant, extract was added to the solution slowly while heating at 60 °C for 5 hr with constant stirring. Then the mixture was settled at room temperature for 24 hr, and the solution was centrifuged for 20 min at 2000 rpm. Then, the solid part was washed with distilled water and ethanol then dried on a ceramic crucible for 24 hr at 70 °C in the oven. Finally, the powder obtained was calcinated and then was kept for further analysis [16].

Characterization of CuO Nps, Co_3O_4, & CuO-Co_3O_4 composite NPs

UV-Vis spectroscopy analysis

The optical properties of biosynthesized CuO NPs, Co_3O_4 NPs, and CuO-Co_3O_4 nano system were characterized by a UV-Vis spectrophotometer. The range of absorption was between 200 nm to 800 nm. In the parabolic band structure, the band gap energy, Eg, and the absorption coefficient of a direct band gap semiconductor are related through Equation (1):

$$(\alpha hv)2 = A(hv - Eg) \quad (1)$$

Where h is Planck's constant, v is the photon's frequency, and A the slope in the linear region. Taking the K-M scattering coefficient S as a constant concerning the wavelength, and using the reflection function in Equation (1), the following expression was derived from Equation (2):

$$(F(R)\ldots)2 = A(hv - Eg) \quad (2)$$

Where, F(R) is equal to K/S, the molar absorption coefficient K is equal to (1 – R)2, the scattering factor S is equal to 2R, and R is the reflectance of the materials and is defined as $\frac{\%R}{100}$. The direct and indirect bandgap energies of the nanomaterials were determined by extrapolation of the linear portion of Kubelka–Munk (K–M) plots [17].

Powder X-ray diffractometer (pXRD) analysis

To determine crystallinity, structure imperfections, and crystallite size of the

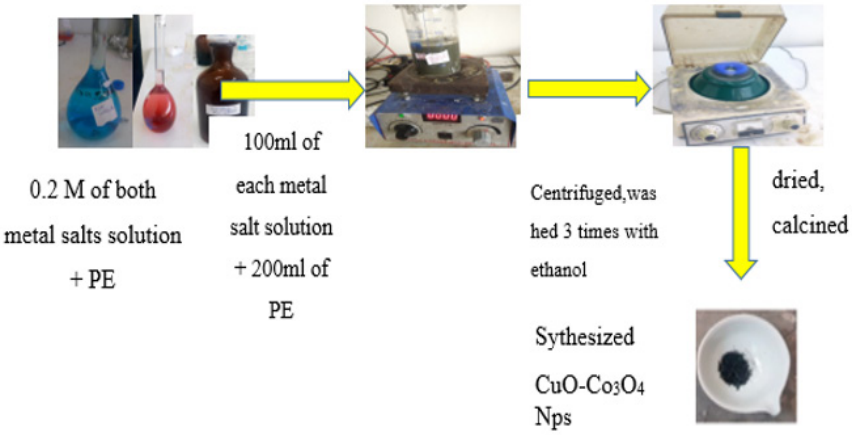

Fig. 5. General procedure for the biosynthesis of copper oxide-cobalt oxide nano system using *M. stenopetala* extract

synthesized CuO Nps, Co_3O_4, and CuO-Co_3O_4 Composite NPs, XRD were examined by using the Shimadzu XRD-700 Powder X-ray diffractometer (pXRD). The x-ray diffraction (PXRD) patterns were recorded at the range of 2θ from 2θ =10° ≤ 2θ ≤ 80° with a scan rate of 20/ min using Cu Kα radiation with an accelerating voltage of 40 KV. The crystallite size D of a particle can be estimated according to the Scherrer equation:

$$D = \frac{K\lambda}{\beta \cos\theta} \quad (3)$$

Here, the x-ray wavelength λ is 0.154 nm, k is the structure factor, which is assigned a value of 0.94, D is the average diameter of the crystals, θ is the Bragg angle in degrees, and β is the full-width at half-height of the prominent peaks.

Scanning electron microscopy (SEM) analysis

The SEM analysis of the biosynthesized CuO NPs, Co_3O_4 NPs, and CuO-Co_3O_4 composite NPs were carried out by using SEM (JCM-6000 plus BENCH TOP SEM, SHIMADZU Corporation, Japan) which reveals information about the external morphology of the biosynthesized CuO Nps, Co_3O_4, and CuO-Co_3O_4 Composite NPs with direct visualization.

Fourier transform infrared (FTIR) analysis

The FTIR analysis of the synthesized nanoparticles was conducted to identify the functional groups involved in the synthesis of the nanoparticles and nanocomposite. FTIR spectrum of the biosynthesized CuO NPs, Co_3O_4 NPs, and CuO-Co_3O_4 composite NPs samples was recorded on FT-IR in the range 4000-400 cm^{-1}.

Thermogravimetric analysis (TGA) analysis

The thermogravimetric analysis of the biosynthesized CuO Nps, and Co_3O_4 Nps were done in a flowing air atmosphere and the thermograms were recorded in the temperature range of 25–800 °C, at a heating rate of 20 °C/min. TGA measures the percent weight loss of a test sample.

Procedure for Antibacterial Activity Test

The synthesized CuO NPs, Co_3O_4 NPs, and CuO-Co_3O_4 nano system were screened for *in vitro* antibacterial activities against four bacteria strains (*E. coli (*Gram-negative), *S. aureus* (Gram-positive), *S. pyogenes* (Gram-positive), and *P. aurus* (Gram-negative)) by Agar disc diffusion method. The bacterial stock cultures were maintained on the sheep blood agar slants at 37 °C. Freshly, grown liquid culture of the test strains having similar turbidity with 0.5 McFarland was seed over the Mueller Hinton agar medium with a sterile swab.

The disc measuring 6 mm in diameter were prepared from Whatman filter paper and sterilized by dry heat at 121 °C for 20 min. The different concentrations of CuO NPs, Co_3O_4 NPs, and CuO-Co_3O_4 nano system (24, 12, 6, and, 3 mg/mL) were prepared by dissolving the synthesized nanoparticles in DMSO. Then, sterilized 6 mm filter paper discs and soaked them in each prepared nanoparticle. The growth inhibition zones were measured in mm after 24 h incubation at 37 °C and compared with the standard drug Gentamicin. DMSO was used as a negative control. All the above procedures were repeated three times and the mean standard deviation of a zone of inhibition were taken [18].

Antioxidant activity Analysis by DPPH scavenging assay

The DPPH scavenging assay was considered an easy as well as cost-effective well-known method for the determination of the antioxidant activity of materials since the radical is stable at room temperature. To study the antioxidant capacity, 1 mL of 10 mg/mL, 20 mg/mL, 30 mg/mL and, 40 mg/mL of each CuO NPs, Co_3O_4 NPs and, CuO-Co_3O_4 nano system were added separately to 1 mL of 0.2 mM Methanolic DPPH solution (by dissolving 3mg of DPPH in 50 mL of methanol), which was added to four different test tubes. The reaction mixture was incubated at room temperature for 30 min. Then the absorbance was recorded at 517 nm using a Shimadzu UV-2550 UV-Visible spectrophotometer. The colour of the DPPH solution eventually turned colourless or pale yellow as the reaction progressed due to the antioxidant activity of the produced nanoparticles. Antioxidant activity (%) of the synthesized nanoparticles was estimated using the following mathematical relation.

$$\%\ \text{Of DPPH scavenging} = \left[\frac{Ac - As}{Ac}\right] \times 100 \quad (4)$$

Where, Ac is the UV-Visible peak intensity at 517 nm for control (DPPH) and As is the UV-Visible peak intensity at 517 nm for the supernatant DPPH solution [19].

RESULTS AND DISCUSSION

The Phytochemical screening test results

The phytochemical screening of extracted *M. stenopetala* leaf plant extracts was carried out

Table 1. Results of phytochemical screening of *M. stenopetala* plant extract

S. no	Secondary Metabolite	Results
1	Flavonoids	+
2	Tannins	+
3	Terpenoid	+
4	Steroid	+
5	Glycosides	+
6	Phytosterols	-
7	Saponins	+
8	Phenols	+

to understand the phytochemicals responsible for the reduction and/or capping of the metal oxides during nanoparticle synthesis. Therefore, the results of the phytochemical analysis of *M. stenopetala* plant extracts are summarized in Table 1 and supported by Fig. 6.

The results gathered showed that the main phytochemical components of the *M. stenopetala* plant extract were flavonoids, tannins, terpenoids, steroids, glycosides, saponins, and phenols, which are supposed to be responsible for aiding in the synthesis of CuO, Co_3O_4, and CuO-Co_3O_4 nano system.

UV-Vis spectroscopy analysis

The optical properties of the biosynthesized CuO NPs, Co_3O_4 NPs, and CuO-Co_3O_4 nano system are shown as follows. Fig. 7 (a and b) shows the absorption spectra and energy band gap for CuO NPs. Fig. 8 (a and b) shows the absorption spectra and energy band gap for Co_3O_4 NPs and similarly, Fig. 9 (a and b) presents the absorption spectra and energy band gap for CuO-Co_3O_4 composite NPs. In the UV-Vis spectrum of the synthesized CuO NPs, the surface plasmon absorption of metal oxide resulted in an absorption peak at 263 nm as shown in Fig. 7(a), no additional peaks were found in the 200-800 nm range and the absorption peak was found to be symmetrical.

The surface plasmon absorption in the metal oxide nanoparticles is based on the collective oscillation of the free conduction band electrons excited by the incident electromagnetic radiation. This type of resonance occurs when the wavelength of the incident light far exceeds the particle diameter. The surface plasmon absorption band with a maximum of 263 nm indicates the

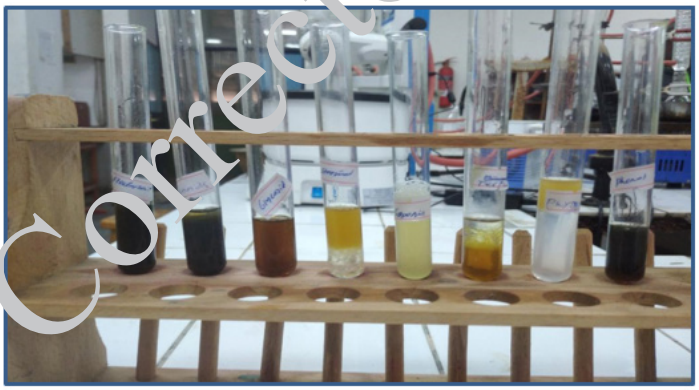

Fig. 6. Results of phytochemical screening of M. stenopetala plant extract.

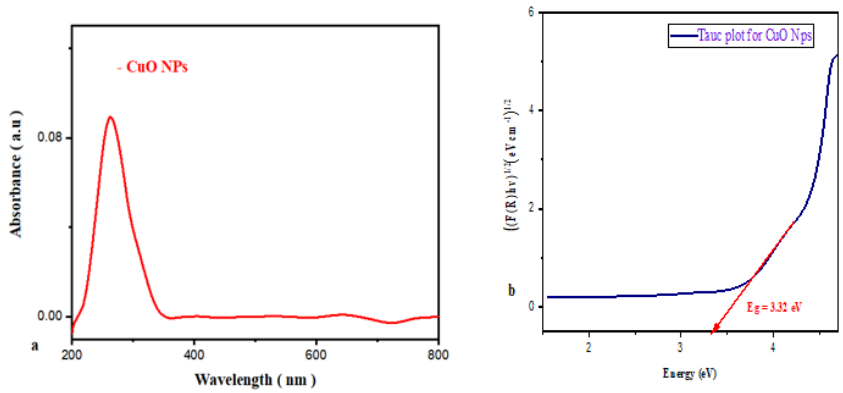

Fig. 7 (a) Wavelength versus Absorbance of UV-Vis spectroscopy, (b) energy versus band gap of CuO NPs.

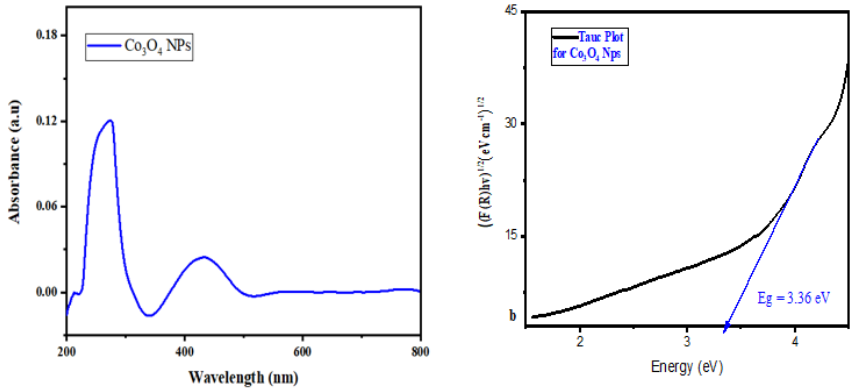

Fig. 8. (a) Wavelength versus Absorbance of UV-Vis spectroscopy, (b) energy versus band

formation of CuO nanoparticles [20].

The obtained result agrees with the reported literature value, for CuO NPs, the surface plasmon resonance is in the range of 200–350nm [21] research institutes and industries. Among all metal oxides, copper oxide nanoparticles (CuO NPs. The results were also in good agreement with the cited study [22]. The bandgap energy for the synthesized CuO NPs was determined by the Tauc relations and the plots were shown in Fig. 7 (b), which indicates the band gap of synthesized CuO Nps is 3.32 eV.

The absorbance and bandgap spectra of Phyto-mediated Co_3O_4 nanoparticles are displayed in Fig. 8 (a and b) with characteristic peaks corresponding to Co_3O_4 nanoparticles observed at around 280 nm and 441 nm. The first broad and the second slightly visible two peaks of Co_3O_4 nanoparticles elucidated the transition of charge from O to Co orbitals. Co^{2+} and Co^{3+} orbital electrons move towards the O^{2-}, which indicates the double oxidation state of cobalt elements.

The calculated band gap of the phyto-mediated Co_3O_4 nanoparticle iis 3.36 eV, which is in agreement with previously reported band gap for Co_3O_4 nanoparticles [23]. The wide band gap of Co_3O_4 nanoparticles explained the gap between the holes and electrons, which suppressed the recombined activity. The obtained photo exciton charge carriers provoke the oxygen vacancy on the Co_3O_4 nanoparticles. The charge carrier mitigations and partings may deduce the organic pollutants and deactivate the bacterial system in wastewater and biomedical applications.

From Fig. 9 (b) the optical energy band gap of CuO-Co_3O_4 composite NPs was found to be 3.66 eV. The optical band gap increased on average in the final composite NPs relative to their monometallic counterpart. This indicates that the composite NPs exhibited strong quantum confinement, which shifts the energy levels of the conduction and valence bands apart and gives rise to a blue shift in the transition energy as the particle size decreases [24].

Powder X-ray diffraction (pXRD) analysis results

Powder XRD analysis was performed to analyse the structure and crystallinity of the synthesized CuO NPs, Co_3O_4 NPs, and CuO-Co_3O_4 composite

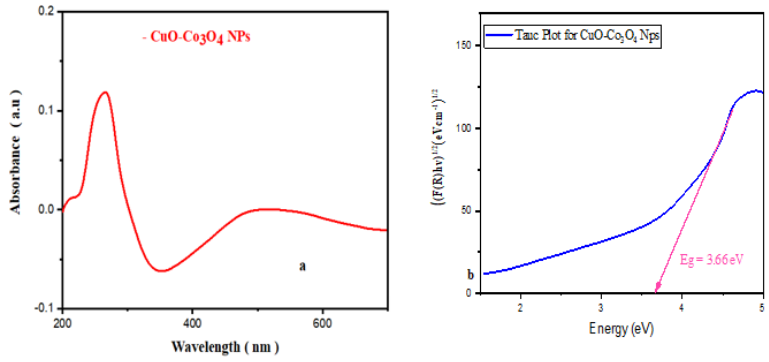

Fig. 9. (a) Wavelength versus Absorbance of UV-Vis spectroscopy, (b) energy versus band the gap of CuO-Co_3O_4 composite NPs

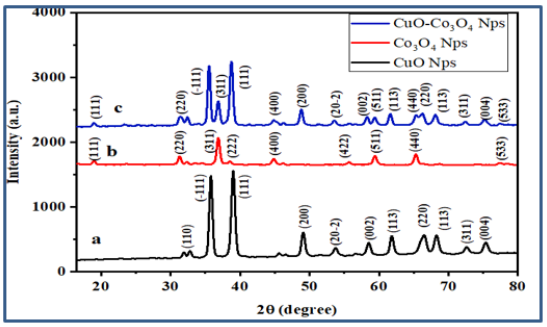

Fig. 10. X-ray diffraction patterns a) CuO NPs, b) Co_3O_4 NPs, and c) CuO-Co_3O_4 composite NPs

NPs. Fig. 10 shows the XRD results of the prepared samples. Experimentally obtained samples were identified by comparison against standard CuO NPs and Co_3O_4 NPs samples. For CuO NPs, diffraction peaks were observed values: 32.7°, 35.8°, 39.02°, 53.75°, 58.52°, 61.85°, 66.38°, 68.28°, 72.6°, and 75.38° which correspond to (110), (-111), (111), (200), (20-2), (002), (113), (220), (113), (311), and (004) planes as shown in Fig. 10 (a). The spectral data showed that the synthesized CuO NPs exhibited a monoclinic phase, and the observed peaks were fitted using the Joint Committee on Powder Diffraction Standard (JCPDS Map #048-1548), space group C2/c), which agrees with that previously reported work [13].

The XRD pattern of Co_3O_4 NPs has been presented in Fig. 10 (b), and in the diffractogram the diffraction peaks were observed at 2θ = 18.99°, 31.31°, 36.88°, 38.43°, 44.86°, 55.69°, 59.42°, 65.30°, and 77.45° corresponding to the miller indices (hkl) values of (111), (220), (311), (222), (400), (422), (511), (440), and (533) respectively. The spectral data obtained showed that the synthesized Co_3O_4 NPs showed cubic spinel crystal structure phase and the observed peaks were fitted with the Joint Committee on Powder Diffraction Standard (JCPDS card No. 042-1467, space group Fd-3m), which is in agreement with the previously reported work [15].

The XRD diffraction pattern of CuO-Co_3O_4 composite NPs is presented in Fig. 10 (c). The peaks at 2θ values 18.99°, 31.37°, 36.85°, 44.68°, 53.54°, 61.60°, 65.90°, 72.40°, 75.10°, and 77.51° corresponding to the miller indices (hkl) values of (111), (220), (311), (400), (200), (002), (440), (311), (004), and (533) respectively. The diffraction peaks at 2θ values of 53.54°, 61.60°, 72.40°, and 75.10° are associated with the (20-2), (113), (311) and (004) planes of monoclinic phase CuO (JCPDS card No. 48-1548), and the peaks at 2θ values 18.99°, 31.37°, 36.85°, 44.68°, 65.90°, and 77.51° correspond to the miller indices of (111), (220), (311), (400), (440), and (533) are planes of Co_3O_4 (JCPDS card No. 042-1467) confirming that the synthesized CuO-Co_3O_4 nanostructures have a crystalline structure.

It can be seen that both CuO and Co_3O_4 peaks can be found in the sample. The relative intensities of the Co_3O_4 peaks decreased compared to those of the CuO peaks due to the formation of the CuO shell coating on the Co_3O_4 core surface.

For the synthesized CuO NPs, Co_3O_4 NPs, and CuO-Co_3O_4 composite NPs the d-spacing (d), particle size (D), dislocation density (δ), and microstrain (ε) were calculated, and presented in the Table (2-4) below for the strongest peaks of respective synthesized NPs.

Based on the above calculation data, one can correlate the peak position (2θ), average crystal size (D) and micro strain (ε), and dislocation density (δ) as follows: The decrease in the microstrain (ε)

Table 2. The calculated parameters for the strongest peaks of CuO NPs

No.	2θ	θ	β	D (nm)	D average (nm)	d- spacing	δ x 10^{-3} (nm^{-2})	ε x 10^{-3}
1	32.7	16.39	0.47	16.08	11.59	2.72	3.86	7.02
2	35.8	17.90	0.50	15.06		2.50	4.40	6.77
3	39.02	19.51	0.59	12.63		2.30	6.26	7.29
4	53.75	26.87	0.53	13.13		1.70	5.79	4.64
5	58.52	29.26	0.56	12.28		1.57	6.62	4.39
6	61.85	30.92	0.54	12.59		1.49	6.30	3.94
7	66.38	33.2	1.02	6.49		1.40	23.71	6.82
8	68.28	34.14	0.70	9.29		1.37	11.57	4.55
9	72.6	36.3	0.21	9.81		1.25	10.85	1.29
10	75.38	37.69	0.73	8.59		1.25	13.54	1.29

The average crystallite size of the CuO NPs was deduced to be 11.59 nm

Table 3. The calculated parameters for the strongest peaks of Co_3O_4 NPs

No.	2θ	θ	β	D(nm)	D average (nm)	d- spacing	δ x 10^{-3} (nm^{-2})	ε x 10^{-3}
1	18.99	9.49	0.49	15.73	12.25	4.66	4.04	13.0
2	31.31	15.65	0.52	14.49		2.85	4.76	8.21
3	36.88	18.44	0.55	13.58		2.43	5.41	7.25
4	38.43	19.21	0.93	8.06		2.34	15.37	11.64
5	44.86	22.43	0.60	12.20		2.01	6.71	6.36
6	55.69	27.84	0.53	13.16		1.64	5.76	4.40
7	59.42	29.71	0.62	11.01		1.55	8.23	4.78
8	65.30	32.65	0.61	10.89		1.42	8.42	4.18
9	77.45	38.72	0.55	11.17		1.23	8.00	3.01

The average crystallite size of the Co_3O_4 NPs was deduced to be 12.25 nm

Table 4. The calculated parameters for the strongest peaks of CuO-Co_3O_4 NPs

No.	2θ	θ	β	D(nm)	D average (nm)	d- spacing	δ x 10^{-3} (nm^{-2})	ε x 10^{-3}
1	18.99	9.49	0.59	13.20	9.53	4.66	5.73	15.48
2	31.37	15.68	1.57	4.85		2.84	42.[illegible]	24.47
3	36.85	18.42	4.90	1.53		2.43	[illegible].18	64.28
4	44.68	22.34	0.99	7.37		2.02	18.38	10.57
5	53.54	26.77	0.49	14.34		1.71	4.85	4.27
6	61.60	30.80	0.52	13.07		[illegible].00	5.85	3.82
7	65.90	32.95	1.18	5.62		[illegible].71	31.59	7.97
8	72.40	36.20	0.47	13.48		1.30	5.49	2.83
9	75.10	37.55	0.60	10.45		1.26	9.14	3.41
10	77.51	38.75	0.54	11.35		1.23	7.75	2.96

The average crystallite size of the CuO-Co_3O_4 NPs was deduced to be 9.53 nm

shows that the angle (2θ) or peak position increased [illegible] nm, respectively. Peak positions (2) are increased in these sequences. Since the dislocation density depends on the particle size, this means that as the particle size increases, the dislocation density decreases. Thus, the dislocation density decreases in the order CuO-Co_3O_4 composite NPs < CuO NPs < Co_3O_4 NPs.

the average crystal size increases with increasing peak position and this shows that crystal size also contributes to peak broadening. Dislocation density measures the number of dislocations in a unit volume of crystalline materials. With the increasing particle size of the nanoparticles, the dislocation density of the crystalline materials decreases.

In other words, as the peak position (angle) increases, the dislocation density of the crystalline particle decreases. The synthesized CuO NPs, Co_3O_4 NPs, and CuO-Co_3O_4 composite NPs have an average crystal size of 11.59 nm, 12.25 nm, and 9.53

Scanning electron microscopy (SEM) analysis

The morphology of the synthesized CuO NPs, Co_3O_4 NPs, and CuO-Co_3O_4 composite NPs are presented in SEM images shown in Fig. 11(a), 11(b), and 11(c) respectively. The SEM image of

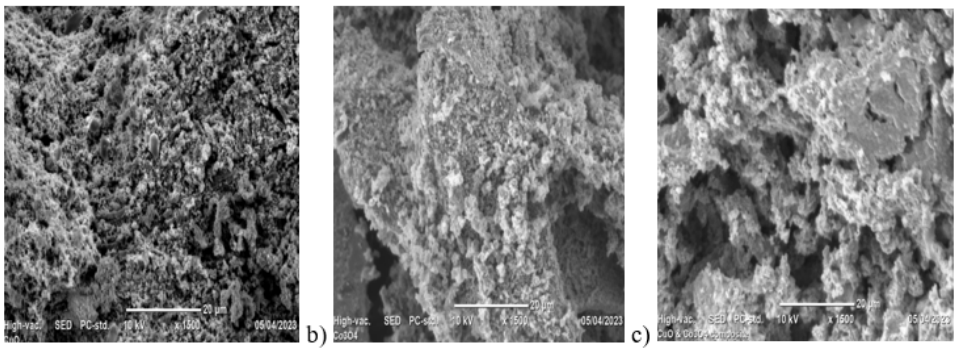

Fig. 11. SEM image of (a) CuO NPs, (b) Co_3O_4 NPs, (c) CuO-Co_3O_4 Nano system

the synthesized CuO NPs is shown in Fig. 11(a). The synthesized CuO NPs exhibited heterogeneous composition. The SEM images show the presence of some large granular particles, which could be due to the aggregation or overlapping of smaller particles associated with the oxidation of nanoparticles. This fact agreed with reports that CuO NPs agglomerate into either clusters or large nanoparticles [26].

The SEM images of Co_3O_4 NPs are shown in Fig. 11(b). The component appears to be agglomerated due to the formation of hydrogen bonds with the molecules surrounded by these active ingredients [23]. It is clear from the SEM image that the components were non-uniformly and agglomerated. This improves the ability of the biosynthesized Co_3O_4 NPs to suppress microorganisms through their smooth surface. On the other hand, the Co_3O_4 nanoparticles had different size particles and irregular geometries, suggesting that they were well dispersed. The SEM image of CuO-Co_3O_4 composite NPs in Fig. 11(c) also revealed the inhomogeneity of the particles in terms of their shape and size. The micrographs show that the CuO-Co_3O_4 composite NPs have both spherical and irregular geometries with different particle sizes in the micrographs.

Fourier transform infrared (FT-IR) spectroscopy analysis

FTIR analysis of the green synthesized CuO NPs, Co_3O_4 NPs, and CuO-Co_3O_4 composite nanoparticles as well as the leaf extract of *M. stenopetala* was performed to reveal the formation of CuO NPs, Co_3O_4 NPs, and CuO-Co_3O_4 composite. This is used to confirm that the bioactive molecules were actively involved during the synthesis process as stabilizing and capping agents to prevent the overall growth of CuO NPs, Co_3O_4 NPs, and CuO-Co_3O_4 composite nanoparticles. Fig. 12 shows the FT-IR result of *M. stenopetala* plant leaf extract and CuO NPs.

The FTIR spectrum for leaf extract of *M. stenopetala* plant Fig. 12 (a) showed the absorption bands at 3437 cm^{-1}, 2901 cm^{-1}, 1606 cm^{-1}, 1383 cm^{-1}, 1008 cm^{-1}, and 572 cm^{-1}. The broad peak observed in the spectrum at around 3437 cm^{-1} confirms the presence of O-H stretching. While the absorption peak located at around 2901 cm^{-1} reveals the presence of C-H stretching vibrations of alkane. A peak at 1606 cm^{-1} showed the presence of carboxyl(C=O) stretch and the observed peak at 1383 cm^{-1} showed an N-H bend of primary amines. The absorptions peak around 1008 cm^{-1} C-O stretch of the ether functional group. The peak at 572 cm^{-1} may correspond to the presence of aryl disulfide (S–S) or polysulfides (S–S stretch) or C–Br stretch [27].

Fig. 12 (b), clearly indicates the peak shifts after the reaction of copper nitrate with leaf extract. The peak shifted, suggesting that the responsible functional groups were involved in the binding mechanism on the CuO NPs. The broad absorption band at 3388 cm^{-1} corresponds to the hydroxyl (OH) functional group in alcohols and phenolic compounds. The peak absorption at 2921 cm^{-1} corresponds to the C-H stretching of Alkane. The IR band around 1612 cm^{-1} can be assigned to the aromatic bending of the alkene group (C=C). The sharp peak at 1383 cm^{-1} is attributed to the deformation vibration of the C–H band of the alkane (CH_3 and CH_2) group. The absorption peak at 1008 cm^{-1} stretching vibration of the C–O group of primary and secondary alcohols (C–O). The peaks around 764, and 537 cm^{-1} correspond to the Cu–O stretching vibration of copper oxide

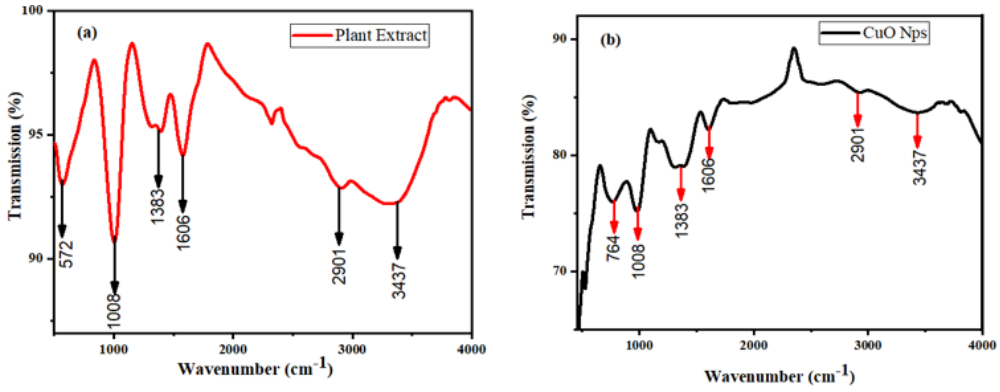

Fig. 12. FTIR spectra of (a) *M. stenopetala* plant extract, (b) CuO NPs

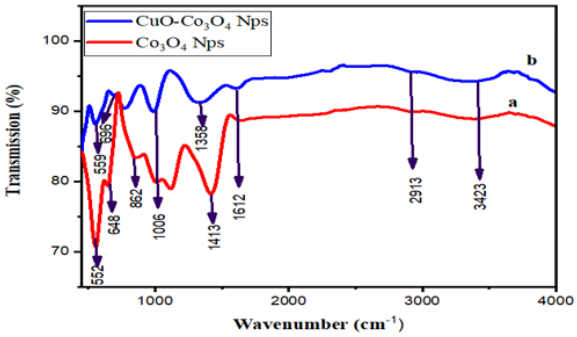

Fig. 13. FTIR spectra of (a) Co_3O_4 NPs, (b) CuO-Co_3O_4 Nano system

nanoparticles in the monoclinic structure[28].

The FTIR spectrum of Co_3O_4 NPs and CuO-Co3O4 composite nanoparticles also showed some shifting in the peaks; peak intensity decreased/ increased, and disappeared. Fig. 18 showed the FT-IR results of Co_3O_4 NPs and CuO-Co_3O_4 composite Nanoparticles. The absorption peaks of Co_3O_4 NPs and CuO-Co_3O_4 composite nanoparticles were observed at 3423 cm^{-1}, 2913 cm^{-1}, 1612 cm^{-1}, 1413 cm^{-1}, 1006 cm^{-1}, 862 cm^{-1}, 648 cm^{-1}, 552 cm^{-1} and 3423 cm^{-1}, 2913 cm^{-1}, 1612 cm^{-1}, 1358 cm^{-1}, 1006 cm^{-1}, 696 cm^{-1}, 559 cm^{-1} respectively.

Fig. 13 (a) indicates the FT-IR spectra of the sample Co_3O_4 NPs exhibit, the absorption peak at 3423 cm^{-1} corresponding to –OH stretching of the carboxylic acid. The absorption peak located at around 2913 cm^{-1} reveals the presence of C-H stretching vibrations of alkane. The peaks located at 1612 cm^{-1} may be due to C=C stretching. The absorption peak revealed at 1413 cm^{-1} and 1006 cm^{-1} corresponds to the N=O Bend of the nitro group and C-O stretch of the ether functional group respectively. Moreover, the peaks at 659 cm^{-1} and 569 showed the stretching vibration of Co–O, corresponding to the tetrahedral and octahedral coordination of Co^{2+} and Co^{3+}, respectively [16, [29, 30].

Fig. 13 (b) shows FT-IR spectra of the sample CuO-Co_3O_4 composite nanoparticles exhibited, band at the band at 3423 cm^{-1} indicating the –OH stretching of the carboxylic acid. The band located at around 2913 cm^{-1} shows the presence of C-H stretching vibrations of alkane. The absorption peak around 1612 cm^{-1} and 1358 cm^{-1} indicated the N=O Stretch of the Nitro group and N=O bending of the nitro group. While the absorption peak at 1006 cm^{-1} indicated the presence of C-O stretch of the ether functional group. The peak at 696 cm^{-1} may correspond to the presence of substituted alkene. The absorption peak at 559 cm^{-1} corresponds to the stretch Co-O present in CuO-Co_3O_4 composite Nanoparticles [25, 30, 20]

Thermogravimetric analysis (TGA/DTA) results

The weight losses of the investigated materials were analysed. Fig. 14 (a) shows the thermal gravimetric analysis and differential thermal analysis of the bio-synthesized CuO NPs. The TGA curve shows the mass loss of the sample, whereas the DTA curve indicates the energy gain or loss during the process. As can be observed from Fig. 14(a), the TGA curve of CuO NPs showed three-step decomposition and weight losses were observed in the temperature ranges of 188.75 °C–402.5 °C, 402.5 °C–514.45 °C, and 515 °C– 600 °C.

The weight loss of the material observed in the temperature range of 188.75 °C – 402.5 °C was about 28.29%, and this was mainly due to the vaporization of water content from the sample. The sample also showed a weight loss of about 15.87% in the temperature range of 402.5 °C–514.45 °C which could be due to the combustion of biomolecules from the *Moringa stenopetala* extract that remained in the biosynthesized NPs. The weight loss observed in

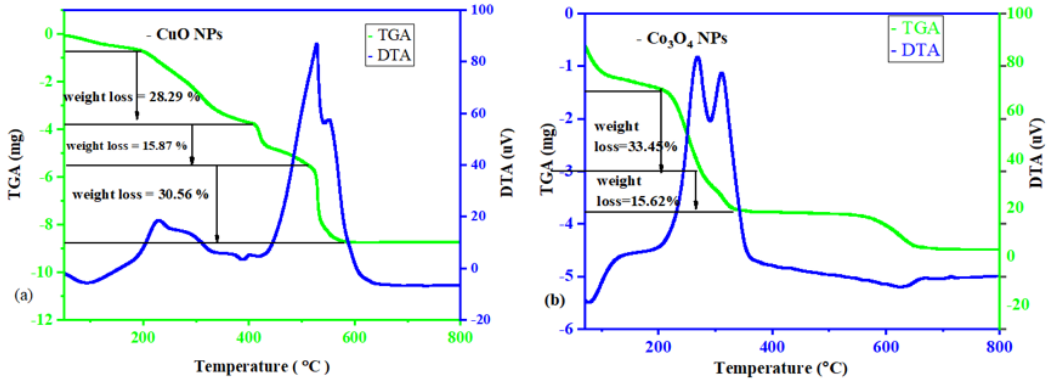

Fig. 14. TGA and DTA results of a) CuO NPs and b) Co_3O_4 NPs

the temperature range of 515 °C–600 °C was about 30.56% which may be due to escaping of oxygen from the sample. In general, from TGA analysis, the total weight loss calculated was 75.33%, and the TGA results suggested that this compound is thermally stable [13].

Fig. 14 (b), shows the thermo gravimetric analysis and differential thermal analysis of the bio-synthesized Co_3O_4 NPs. For Co_3O_4 NPs weight loss of 49.07% was observed from room temperature to 340 °C. The first 33.45% could be due to the loss of residual ethanol or absorbed moisture. The second weight loss 15.62% could be due to the loss of oxygen, enhancing the formation of oxygen vacancies. The weight loss is due to the thermal decomposition or dehydration of Co_2O_4 to Co_3O_4 particles.

Antibacterial activity of synthesized nanoparticles

In this section, the antibacterial activities of the synthesized NPs were discussed. The antibacterial activity of synthesized CuO NPs, Co_3O_4 NPs, and CuO-Co_3O_4 composite NPs with *M. stenopetala* leaf extract was investigated using the agar disk diffusion method. Fig. 15- 17 show,

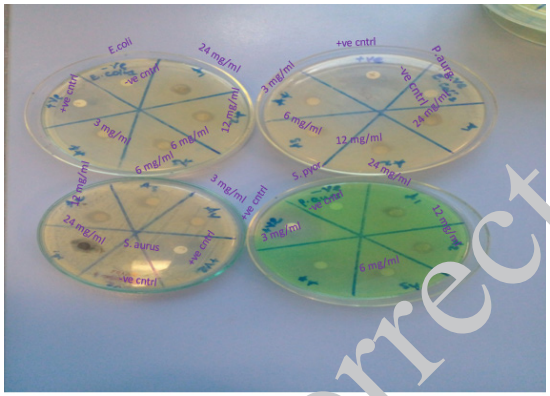

Fig. 15. Antibacterial activities of CuO NPs against gram-negative *Escherichia coli* and *Pseudomonas aeruginosa* and gram-positive *Staphylococcus aureus* and *Streptococcus pyogenes*

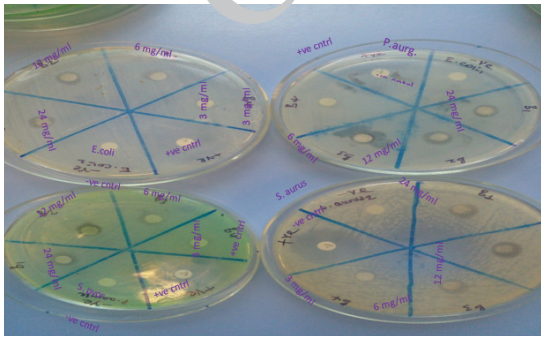

Fig. 16. Antibacterial activities of Co_3O_4 NPs against gram-negative *Escherichia coli* and *Pseudomonas aeruginosa* and gram-positive *Staphylococcus aureus* and *Streptococcus pyogenes*

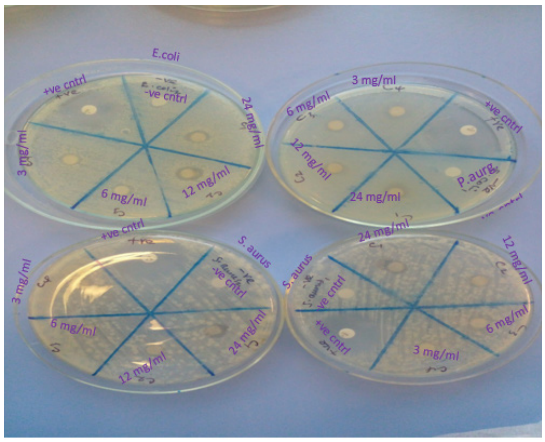

Fig. 17. Antibacterial activities of CuO-Co_3O_4 nano system against gram-negative *Escherichia coli* and *Pseudomonas aeruginosa* and gram-positive *Staphylococcus aureus* and *Streptococcus pyogenes*

the antibacterial activity of the synthesized CuO NPs, Co_3O_4 NPs, and CuO-Co_3O_4 composite NPs against the bacterial strains gram-negative *E. coli* (ATCC25922) and *P. aeruginosa* (ATCC27853), and gram-positive *S. aureus*(ATCC25923) and *S. pyogenes* (ATCC19615).

The antibacterial activity of the synthesized CuO NPs, Co_3O_4 NPs, and CuO-Co_3O_4 nano system against the bacterial strains gram-negative *E. coli* and *P. aeruginosa* and gram-positive *S. aureus* and *S. pyogenes* were tabulated and discussed in Tables (5, 6 and 7) respectively.

As shown in Fig. (15, 16, and 17) supported by Tables (5, 6, and 7), the antibacterial activity of the synthesized CuO NPs, Co_3O_4 NPs, and CuO-Co_3O_4 nano system was enhanced with increasing concentration of the nanoparticles. The presence of an inhibition zone indicates that the mechanism of biocidal action of the synthesized nanoparticles involves the destruction of the cell membrane of bacterial species and eventually leads to the death of pathogens. Thus, the size of the zone of inhibition varied depending on the type of pathogens, the concentration of synthesized nanoparticles, and the type of nanoparticles.

Comparing the antibacterial activity of synthesized CuO NPs, Co_3O_4 NPs, and CuO-Co_3O_4 composite NPs against selected bacterial strains *E. coli, P. aeruginosa, S. aureus,* and *S. pyogenes*, the CuO-Co_3O_4 composite NPs showed the best inhibitory activities against the selected bacterial species (*E. coli, P. aeruginosa,* and *S. pyogenes*) than the inhibitory activities of CuO NPs and Co_3O_4 NPs. However, CuO NPs showed the best

Table 5. Zones of inhibition of CuO NPs and Gentamicin (+ve control) with different concentrations against different bacterial strains

Sample	Concentration(mg/mL)	Zone of Inhibition (mm)			
		Gram-negative species		Gram-positive species	
		E. coli	*P. aeruginosa*	*S. aureus*	*S. pyogenes*
CuO NPs	24	11.06 ± 0.25	12.2 ± 0.7	13.6 ± 0.5	11.3 ± 0.5
	12	10.1 ± 0.1	11.66 ± 0.5	12.66 ± 0.5	10.5 ± 0.25
	6	8.66 ± 0.5	11 ± 0.5	11.8 ± 0.3	8.83 ± 0.45
	3	7.66 ± 0.5	9.33 ± 0.5	11.13 ± 0.3	7.5 ± 0.75
Gentamicin (+ve) control		16 ± 0.25	16 ± 0.3	16 ± 0.1	16 ± 0.1
DMSO (-ve) control		6	6	6	6

Table 6. Zones of inhibition of Co_3O_4 NPs NPs and Gentamicin (+ve control) with different concentrations against different bacterial strains

Sample	Concentration(mg/mL)	Zone of Inhibition (mm)			
		Gram-negative species		Gram-positive species	
		E. coli	*P. aeruginosa*	*S. aureus*	*S. pyogenes*
Co_3O_4 NPs	24	11.66 ± 0.25	13.66 ± 0.5	11 ± 0	11.34 ± 0.65
	12	10.1 ± 0.1	12.4 ± 0.1	10.1 ± 0.25	10.66 ± 0.5
	6	8.66 ± 0.5	11.83 ± 0.25	5 ± 0.25	8.8 ± 0.65
	3	7.7 ± 0.55	10.66 ± 0.5	7.66 ± 0.5	7.83 ± 0.25
Gentamicin (+ve) control		16 ± 0.1	16 ± 0.5	16 ± 0.3	16 ± 0.1
DMSO (-ve) control		6	6	6	6

Table 7. Zones of inhibition of CuO-Co_3O_4 nano system and Gentamicin (+ve control) with different concentrations against different bacterial strains

Sample	Concentration (mg/mL)	Zone of Inhibition (mm)			
		Gram-negative species		Gram-positive species	
		E. coli	*P. aeruginosa*	*S. aureus*	*S. pyogenes*
CuO-Co_3O_4 Composite NPs	24	15	14.66 ± 0.5	13	12.66 ± 0.5
	12	13.73 ± 0.6	13.5 ± 0.75	11.76 ± 0.65	11.7 ± 0.55
	6	12.76 ± 0.65	12.6 ± 0.9	10.8 ± 0.7	10.7 ± 0.6
	3	11.46 ± 0.7	11.23 ± 0.35	9.83 ± 0.75	9.76 ± 0.65
Gentamicin (+ve) control		18 ± 0	18± 0.1	18 ± 0	18 ± 0
DMSO (-ve) control		6	6	6	6

inhibitory effects against bacterial species (*S. aureus*) that were not both Co_3O_4 NPs and CuO-Co_3O_4 nano system, and Co_3O_4 NPs showed the best inhibitory effects against selected bacterial species (*E. coli, P. aeruginosa,* and *S. pyogenes*), except CuO NPs. and CuO NPs showed the lowest inhibitory activity against the selected bacterial species (*E. coli, P. aeruginosa,* and *S. pyogenes*) compared to Co_3O_4 NPs and CuO-Co_3O_4 nano system. The result obtained from research has a strong agreement with previous literature, it can be an indication of the validity and reliability of the research findings. It means that the results are consistent with the existing body of knowledge in the field and support the current understanding of the topic [31, 32].

Antioxidant activity of the synthesized Nanoparticles

DPPH possesses stable free radicals with an unpaired electron, causing its deep purple colour. Electron-rich compounds can donate electrons, reducing DPPH and causing a colour change from violet to yellow. This reduction disrupts DPPH's conjugation, converting it into a non-magnetic molecule. The resulting discoloration

is stoichiometric in relation to the number of electrons accepted [19]. The antioxidant activity of the biosynthesized nanoparticles was investigated at different concentrations ranging from 10-40 mg/mL. As the surface reactions between synthesized nanoparticles (CuO NPs, Co_3O_4 NPs, and CuO-Co_3O_4 nano system), and the DPPH solution proceeded, the colour of the solution slowly changed from deep violet to pale yellow. A gradual increase in the peak intensity of the synthesized nanoparticle solution at 517 nm with increasing concentration was observed by UV-Vis analysis (Fig. 18).

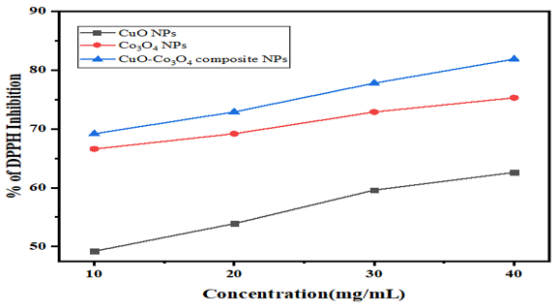

Fig. 18. Comparative graph of DPPH assay study results of CuO NPs, Co_3O_4 NPs, and CuO-Co_3O_4 nano system at different concentrations

The colour change of the DPPH solution as well as the magnitude of the increase in the UV-visible peak intensity in the presence of CuO NPs, Co_3O_4 NPs, and CuO-Co_3O_4 nano system gives the visual monitoring of the antioxidant activity of the synthesized nanoparticles. By determining the UV-visible peak intensity of the control and the considered supernatant solution at different concentrations, the percentage of antioxidant activity of the synthesized nanoparticles when varying the concentration was given in Fig. 18, which shows a gradual increase in antioxidant activity with increasing concentration CuO NPs, Co_3O_4 NPs, and CuO-Co_3O_4 composite NPs. The results of the DPPH inhibition study are shown in Table 8 and the comparative graph is shown in Fig. 19. The DPPH radical test of CuO NPs, Co_3O_4 NPs, and CuO-Co_3O_4 nano system were compared to each other. The results confirm that the CuO-Co_3O_4 nano system have the best and highest DPPH inhibitory activity compared to CuO NPs and Co_3O_4 NPs and that the Co_3O_4 NPs also showed increased radical inhibitory activity than CuO NPs compared to the green synthesized CuO NPs showed the lowest antioxidant activity. At a concentration of 40 (mg/mL), a scavenging capacity of CuO-Co_3O_4 nano system of up to 81.9% was achieved. This shows that synthetic CuO-Co_3O_4 nano system exhibited the highest antioxidant activity. This result agreed with a previous literature [31, 32].

CONCLUSION

In conclusion, the green synthesis of CuO NPs, Co_3O_4 NPs, and CuO-Co_3O_4 nano system using *M. stenopetala* leaf extract as a reducing agent presents a significant advancement in the field of nanotechnology. This approach offers a sustainable and environmentally friendly method for synthesizing nanoparticles with unique properties. The CuO-Co_3O_4 nano system, with its combined composition and synergistic effects, exhibits superior characteristics and advantages over other synthesized nanoparticles. These nanoparticles demonstrate enhanced inhibitory and radical inhibitory activity, making them promising candidates for various applications in fields such as medicine, catalysis, and materials science. Furthermore, their high surface area-to-volume ratio enables efficient interactions with molecules and biological systems, expanding their potential for biomedical and environmental applications. The green synthesis method employed in this study not only ensures minimal environmental impact but also showcases the potential for sustainable and eco-friendly approaches in nanomaterial synthesis. Overall, this research contributes to the broader understanding and utilization of nanotechnology, paving the way for exciting advancements and practical applications in diverse fields.

ACKNOWLEDGEMENTS

The authors would like to acknowledge Adama

Table 8. Results obtained in DPPH radical scavenging assay

S. No	Concentration (mg/mL)	% Of DPPH Inhibition		
		CuO NPs	Co_3O_4 NPs	CuO-Co_3O_4 Composite NPs
1	10	49.2	66.6	69.2
2	20	53.9	69.2	72.9
3	30	59.6	72.9	77.8
4	40	62.6	75.3	81.9

Science and Technology University for supporting this research.

FUNDING

This work is financially supported by Adama Science and Technology University and the Ministry of Innovation and Technology of Ethiopia under the grant number ASTU/SM-R/684/23, Adama, Ethiopia.

CONFLICTS OF INTEREST

The authors declare that they have no any conflict of interest.

REFERANCES

1. Whitesides GM. Nanoscience, nanotechnology, and chemistry. Small. 2005;1(2):172-179.
2. Mansoori GA, Soelaiman TAF. Nanotechnology, An Introduction for the Standards Community. Nanomedicine (Lond). 2005;2(6):1-21.
3. Mungondori HH, Ramujana S, Katwire DM, Taziwa RT. Synthesis of a novel visible light responsive γ-Fe2O3/SiO2/C-TiO2 magnetic nanocomposite for water treatment. Water Sci Technol. 2018;78(12):2500-2510.
4. Mauricio MD, Marchio P, Valles SL, Aldasoro M, Herance JR, Rocha M, et al. Review Article Nanoparticles in Medicine: A Focus on Vascular Oxidative Stress. Oxid Med Cell Longev. 2018;(8):3-4.
5. Rastogi A, Tripathi DK, Yadav S, Chauhan DK, Živčák M, Ghorbanpour M, et al. Application of silico nanoparticles in agriculture. Biotech. 2019;9(3):90
6. Zhang D, Ma X, Gu Y, Huang H, Zhang G. Green Synthesis of Metallic Nanoparticles and Their Potential Applications to Treat Cancer. Front Chem. 2020; (8): 799
7. Mutukwa D, Taziwa R, Khotseng LE. A Review of the Green Synthesis of ZnO Nanoparticles Utilising Southern Africa Indigenous Medicinal Plants. Nanomaterials. 2022; 12(19), 3456.
8. Riaz T, Nayyar S, Shahzadi T, Zaib M, Shahid S, Mansoor S, et al. The Biogenic Synthesis of Cobalt Monometallic and Cobalt-Zinc Bimetallic Nanoparticles Using Cymbopogan citratus L. Leaf Extract and Assessment of Their Activities as Efficient Dye Removal and Antioxidant Agents. Research Gate. 2022 Oct;12(10):2505.
9. Awad AM, Kumar P, Ismail-Fitry MR, Jusoh S, Ab Aziz MF, Sazili AQ. Green extraction of bioactive compounds from plant biomass and their application in meat as natural antioxidant. Antioxidants. 2021;10(9):1-39.
10. Demssie Dejen K, Kibret DY, Mengesha TH, et al. Green synthesis of silver and cobalt oxide nanoparticles using Croton macrostachyus plant extract and evaluation of their antibacterial activity. 2024;11(1):80-92.
11. Shehu Z, Lamayi W, Danbature D+, Magaji B, Muhammad, Adam M, et al. Green Synthesis and Nanotoxicity Assay of Copper-Cobalt Bimetallic Nanoparticles as a Novel Nanolarvicide for Mosquito Larvae Management. Int J Biotechnol. 2020;9(2):99-104.
12. Panchal P, Parvez N. Phytochemical analysis of medicinal herb (Ocimum sanctum). Int J Nanomater Nanotechnol Nanomedicine. 2019;5(2):8-11.
13. Andualem WW, Sabir FK, Mohammed ET, Belay HH, Gonfa BA. Synthesis of copper oxide nanoparticles using plant leaf extract of Catha edulis and its antibacterial activity. J Nanotechnol. 2020;(20):1-10
14. Benhammada A, Trache D. Green synthesis of CuO nanoparticles using Malva sylvestris leaf extract with different copper precursors and their effect on nitrocellulose thermal behavior. J Therm Anal Calorim. 2022;147(2):1355-1370.
15. Govindasamy R, Raja V, Singh S, Govindarasu M, Sabura S, Rekha K, Rajeswari VD, Alharthi SS, Vaiyapuri M, Sudarmani R, Jeyarani S, Venkidasamy B, et al. Green Synthesis and Characterization of Cobalt Oxide Nanoparticles Using Psidium guajava Leaves Extracts and Their Photocatalytic and Biological Activities. Molecules. 2022;27(17):1-16.
16. Aragaw SG, Sabir FK, Endoshe DM, Zelekew OA. Green synthesis of p-Co_3O_4/n-ZnO composite catalyst with Eichhornia crassipes plant extract mediated for methylene blue degradation under visible light irradiation. Mater Res Express. 2020;7(5):1-11
17. Abebe B, Murthy HCA, Zereffa EA, Adimasu A. Synthesis and characterization of ZnO/PVA nanocomposites for antibacterial and electrochemical applications. Inorg Nano-Metal Chem. 2021;51(8):1127-1138.
18. Gopinath K, Kumaraguru S, Bhakyaraj K, Mohan S, Venkatesh KS, Esakkirajan M, et al. Green synthesis of silver, gold, and silver/gold bimetallic nanoparticles using the Gloriosa superba leaf extract and their antibacterial and antibiofilm activities. Microb Pathog. 2016 ;(101):1-11.
19. Das D, Jyoti B. Synthesis, characterization and biological applications of cobalt oxide (Co_3O_4) nanoparticles. Chem Phys Impact. 2023;6(December 2022):100137.
20. Naika HR, Lingaraju K, Manjunath K, Kumar D, Nagaraju G, Nagabhushana H. Green synthesis of CuO nanoparticles using Gloriosa superba L. extract and their antibacterial activity. Integr Med Res. 2018;9(1):7-12.
21. Akintelu SA, Folorunso AS, Folorunso FA, Oyebamiji AK. Green synthesis of copper oxide nanoparticles for biomedical application and environmental remediation. Heliyon. 2020;6(7):04508.
22. Shelke HD, Machale AR, Survase AA, Pathan HM, Lokhande CD, Lokhande AC, Shaikh SF, Rana AuHS, Palaniswami M.. Multifunctional Cu2SnS3 nanoparticles with enhanced photocatalytic dye degradation and antibacterial activity. Materials. 2022; (9):15.
23. Govindasamy R, Raja V, Singh S, Govindarasu M, Sabura S, Rekha K, Rajeswari VD, Alharthi SS, Vaiyapuri M, Sudarmani R, et al. Green synthesis and characterization of cobalt oxide nanoparticles using Psidium guajava leaves extracts and their photocatalytic and biological activities. Molecules. 2022. (17):27.
24. Meghdadi S, Amirnasr M, Zhiani M, Jallili F, Jari M, Kiani M. Facile synthesis of cobalt oxide

nanoparticles by thermal decomposition of cobalt(II) carboxamide complexes: Application as oxygen evolution reaction electrocatalyst in alkaline water electrolysis. Electrocatalysis. 2017;8(2):122-131.
25. Das D, Nath BC, Phukon P, Dolui SK. Synthesis and evaluation of antioxidant and antibacterial behavior of CuO nanoparticles. Colloids Surfaces B Biointerfaces. 2013;(101):430-433.
26. Krishna BA, Kumar PN, Prema P. Green synthesis of copper oxide nanoparticles using Cinnamomum malabatrum leaf extract and its antibacterial activity. Indian J Chem Technol. 2020;27(6):525-530.
27. Dalvand A, Gholami M, Mahvi AH, Dehghani MH, Dalvand K, Jafari AJ, et al. Comparison of Moringa stenopetala seed extract as a clean coagulant with Alum and Moringa stenopetala-Alum hybrid coagulant to remove direct dye from Textile Wastewater. Environ Sci Pollut Res Int. 2016;23(16):16396-405.
28. Varughese A, Kaur R, Singh P. Green synthesis and characterization of copper oxide nanoparticles using Psidium guajava leaf extract. IOP Conf Ser Mater Sci Eng. 2020; 961(1):012011.
29. Diallo A, Beye AC, Doyle TB, Park E, Maaza M. Green synthesis of Co_3O_4 nanoparticles via Aspalathus linearis: Physical properties. Green Chem Lett Rev. 2015;(8):3-4, 30-36.
30. Bhargava R, Khan S, Ahmad N, Mohsin M, Ansari N. Investigation of structural, optical and electrical properties of Co_3O_4 nanoparticles. AIP Conf Proc. 2018;(030034): 1–5
31. Peddi P, Ptsrk PR, Rani NU, Tulasi SL. Green synthesis, characterization, antioxidant, antibacterial, and photocatalytic activity of *Suaeda maritima* (L.) Dumort aqueous extract-mediated copper oxide nanoparticles. J Genet Eng Biotechnol. 2021;(19):1
32. Hajri AK, Albalawi MA, Alsharif I, Jamoussi B. Marine algae extract (Grateloupia sparsa) for the green synthesis of Co_3O_4 NPs: Antioxidant, antibacterial, anticancer, and hemolytic activities. Bioinorg Chem Appl. 2022; (2022): 1–11.